Effect of Thickness on Crystal Structure and Dispersion Parameters of Haematite Iron Oxide by Spray Pyrolysis Technique

Ahmed T. Hassan[a] and Ehssan S. Hassan[b,*]

[a]*Ministry of Education, Directorate General for Education, Iraq, Baghdad*
[b]*Department of Physics, College of Science, Mustansiriyah University, Baghdad, Iraq*

Doi: 10.12693/APhysPolA.140.295　　　*e-mail: ehsanphysicyan@uomustansiriyah.edu.iq

Thin films of haematite iron oxide Fe_2O_3 (of thicknesses $t = 200$, 300, and 400 nm) were prepared on glass substrates using a spray pyrolysis technique. X-ray diffraction measurements showed that the films were polycrystalline, with crystallite size increasing from 16.8 to 30.7 nm as the sample thickness increased. The refractive index data was used to calculate the single oscillator power and scattering energy as predicted by the Wemple–Domenico model. The dispersion energy increased from 10.86 to 16.54 eV as the thickness increased. The optical energy gap decreased from 2.74 to 2.21 eV. The calculated values for the Urbach energy were found to increase from 680 to 1230 meV as the thickness increased.

topics: Urbach energy, transmittance, absorption coefficient

1. Introduction

Haematite iron oxide (Fe_2O_3) has an average direct optical energy gap $E_g = 2$ eV. Al-Kuhaili et al. [1] showed that α-Fe_2O_3 films exhibit the presence of both direct and indirect band gaps. The direct band gap had a value of 2.18 eV for both types of films investigated. The energy of the indirect band gap was 1.82 eV for the films deposited on unheated substrates and 1.96 eV for the films deposited on heated substrates [1]. Thin films are low in cost, stable in aqueous solution, and non-toxic. Thin films can be used in gas sensors [2, 3] due to their high sensitivity to combustible gases, and as radiation filters in the visible region of the electromagnetic spectrum. The Fe_2O_3 thin films have been produced using methods such as pulsed laser deposition, atomic layer deposition [4], spray pyrolysis technique (SPT), RF magnetron sputtering, and the sol–gel method [5, 6]. The model suggested by Wemple and DiDomenico to describe the dispersion of the refractive index of solids is further developed in terms of the cation local bonding environment and its effect on the value of the dispersion energy. In this work, SPT was adopted to deposit Fe_2O_3 thin films.

The objective of this study is to assess the effect of film thickness on the dispersion parameter of Fe_2O_3 thin films deposited by SPT. The process of calculating the optical energy gap, the Urbach energy, the dispersion energy, and the refractive index from the transmittance values will be of interest to researchers.

2. Materials and methods

Spray pyrolysis was undertaken using a standard laboratory glass spray bottle with a yield needle with a span of 1 mm. The volume of the solvent used for deposition was 100 ml. The preliminary solution was sprayed onto a preheated square glass plate of 25.5 mm dimensions and 0.7 mm thickness using compressed air. The solvent flow rate was 8 ml/min and the distance from the needle to the substrate was 30 cm. The technique involves spraying cycles of 5 s followed by a 1 min pause, to avoid sudden cooling of the substrate. The substrates were installed on red of a heater and their temperature was controlled with a thermocouple (chromel–alumel) to keep them at an optimized temperature of 450°C. Hydrated haematite chloride ($FeCl_3 \cdot 6H_2O$) of 162.21 g/mol molecular weight was used for the preparation of the Fe_2O_3 thin films. The solution was prepared at room temperature with concentration of 0.1 M by dissolving 1.6221 g of $FeCl_3 \cdot 6H_2O$ in 100 ml of distilled water. To ensure full solubility a magnetic stirrer was used. After deposition, the films were allowed to cool slowly to ambient temperature. Thickness measurements for the as-deposited thin films were carried out by weighing. The structural properties were measured with X-ray diffraction (XRD, Shimadzu XRD-6000, using Cu K_α radiation of a wavelength of 1.5406 Å) and a UV/visible scanning spectrophotometer (Shimadzu UV-1800) was used to record the absorbance spectra in the wavelength range of 300–900 nm.

3. Results and discussion

Figure 1a presents the X-ray diffraction patterns of Fe_2O_3 deposited by SPT on glass substrates at different thicknesses t, i.e., 200, 300, and 400 nm. The diffraction patterns in Fig. 1 show that the films are polycrystalline. We observed also that the highest reflection intensity in all layers stems from the (220) plane at an angle $2\theta = 30.121°$ and that the full width at half maximum (FWHM) decreases with increasing film thickness. The latter indicates an increase in crystallite size from 16.89 nm to 30.78 nm as the sample thickness increases from 200 nm to 400 nm, as shown in Fig. 1b. Also, secondary (331), (421), and (521) reflexes at $2\theta = 38.121°$, $2\theta = 38.121°$, and $2\theta = 38.121°$, respectively, are observed. All positions agree with those of the international card JCPDS (Card No. 39-1346).

Table I shows the structural parameters of Fe_2O_3 thin films prepared by SPT. The crystallite size D [nm] is calculated using [7, 8]

$$D = \frac{K\lambda}{\beta \cos(\theta)}, \qquad (1)$$

where K is a dimensionless shape factor, λ is the X-ray wavelength (1.54178 Å), β is the line width at half the maximum intensity, and θ is the Bragg angle. The lattice parameters, in turn, are calculated using [7, 8]

$$\frac{1}{d_{hkl}} = \frac{h^2}{a^2} + \frac{k^2}{b^2} + \frac{l^2}{c^2}, \qquad (2)$$

where h, k, and l are the Miller indices, a, b, and c are the lattice parameters, and d_{hkl} is the interplanar distance.

Figure 2 presents the transmittance spectra of the samples prepared with different thicknesses ($t = 200$, 300, and 400 nm) deposited on glass substrates using SPT. Transmittance increases with wavelength growth. This increase is due to the fact that the cross-section area of the dispersed incident rays reduces [9, 10].

The value of the absorption coefficient α can be calculated with

$$\alpha = \frac{2.303A}{t}, \qquad (3)$$

where A is the absorbance and t is the film thickness. It is seen in Fig. 2, that both quantities, t and T, are depended in our system on the considered wavelength. Thus, there is a non-trivial relation between the transmittance and absorbance. It is indicated in further results in this paper.
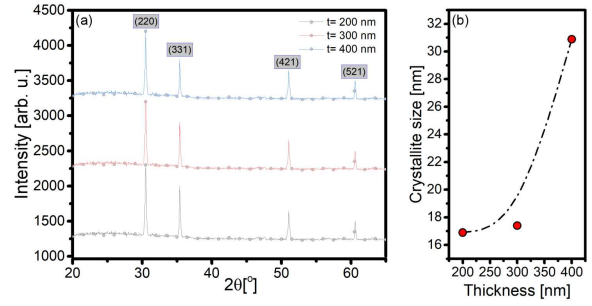
Fig. 1. (a) X-ray diffraction pattern and (b) crystallite size for Fe_2O_3 deposited on glass substrate by SPT.
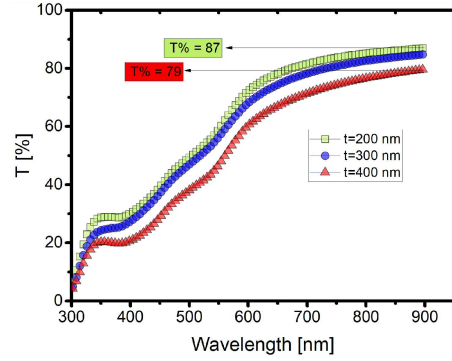
Fig. 2. Transmittance spectrum of Fe_2O_3 deposited on glass substrates by SPT.

Structural parameters of Fe_2O_3 thin films prepared by SPT technique.

TABLE I

Thickness [nm]	(hkl) plane	FWHM [deg]	2θ XRD	2θ ASTM	XRD d [Å]	Crystallite size D [nm]	Lattice parameter [nm]
200	(220)	0.374	30.12	30.241	0.208	16.89	0.4174
	(311)		35.92	35.630			
	(421)		50.23	50.007			
	(521)		59.56	60.685			
300	(220)	0.350	30.23	30.241	0.210	17.39	0.4204
	(331)		35.57	35.630			
	(421)		50.81	50.007			
	(521)		59.92	60.685			
400	(220)	0.342	30.38	30.241	0.208	30.88	0.4170
	(331)		35.73	35.630			
	(421)		50.16	50.007			
	(521)		59.99	60.685			

The optical variables of Fe_2O_3 thin films.

TABLE II

Thickness [nm]	E_g^{opt} [eV]	E_o [eV]	E_d [eV]	E_U [meV]	ε_0	n_0	M_{-1}	M_{-3} [eV^{-2}]	S_o [$\times 10^{-3}$ m^{-2}]	λ_o [nm]
200	2.74	2.22	10.86	680	5.89	2.42	4.89	0.99	2.21	534
300	2.48	2.16	13.89	790	7.43	2.73	6.43	1.37	3.71	512
400	2.21	2.21	16.54	1230	8.48	2.91	7.48	1.53	3.95	526
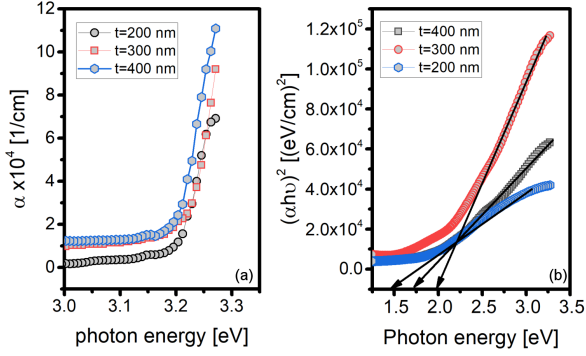
Fig. 3. Absorption coefficient α (a) and $(\alpha h\nu)^2$ (b) as a function of photon energy $h\nu$ of Fe_2O_3 deposited by SPT.

Fig. 4. The logarithm $\ln(\alpha)$ as a function of energy $h\nu$ calculated for Fe_2O_3.

The absorption coefficient α increases with the photon energy, as shown in Fig. 3a.

The relation between the absorption coefficient and the photon energy is given by the Tauc equation

$$\alpha h\nu = B\left(h\nu - E_g^{opt}\right)^n, \tag{4}$$

where B is a constant, E_g^{opt} is the optical band gap energy, $h\nu$ is the photon energy, α reads as $\alpha(\nu)$, and n is an index that depends on the kind of transition (direct or indirect). In the case a of direct transition the appropriate index is $n = 1/2$. The optical band gap energy can be determined from the dependence of $(\alpha h\nu)^2$ vs $h\nu$ by linear extrapolation of the curves towards the $(\alpha h\nu)^2 = 0$ axis.

Figure 3b shows the variation in the optical energy gap for different thicknesses values. The reduction in straight band gap as thickness increases can be attributed to an increase in crystallization as well as an increase in crystallite (grain) size. Absorption near the edge of the basic absorption coefficient is largely dependent on the energy of the photons, the Urbach energy enters through the following relationship [11]

$$\alpha = \alpha_0 \exp\left(\frac{h\nu}{E_U}\right). \tag{5}$$

Taking the natural logarithm of (5), one gets

$$\ln(\alpha) = \ln(\alpha_0) + \left(\frac{h\nu}{E_U}\right) \tag{6}$$

where α_0 is constant, and E_U is the Urbach energy. The linear relation between $\ln(\alpha)$ and the photon energy is expected. In Fig. 4, we can determine the Urbach energy for it is equal to the inverse of the slope of the straight line. The obtained E_U values are shown in Table II. The Urbach energy levels

increase with the thickness of the films. The increase in E_U is credited to the increase in mass as the films increase in thickness. The dispersal of refractive index of Fe_2O_3 films, modelled by the single oscillator, is articulated by Wemple and DiDomenico [12]. The refractive index has been examined in the interband absorption boundary [13]

$$n^2 = 1 + \frac{E_d E_o}{E_o^2 - (h\nu)^2}. \tag{7}$$

Now, one can rewrite (7) as follows

$$\left(n^2 - 1\right)^{-1} = \frac{E_o}{E_d} - \frac{(h\nu)^2}{E_d E_o}, \tag{8}$$

where E_o is the typical oscillator energy (typical of the visual band gap) and E_d is the dispersal energy factor of the objects [14]. The dependence $(n^2 - 1)^{-1}$ against $(h\nu)^2$, shown in Fig. 5, allows to determine the oscillator constant when assigning a linear role to the ratio of E_o and E_d, i.e., E_o/E_d. The values of the parameter E_o/E_d and the slope $1/(E_o E_d)$ that describe the dependence of single effective oscillator parameters on thickness, are shown in Table I. The static refractive index n_0 is evaluated as follows $n_0^2 = n^2(h\nu = 0) = 1 + \frac{E_d}{E_o}$, and the infinite wavelength dielectric constant is given by $\varepsilon_0 = n_0^2$. The obtained values are shown in Table II.

The moments of visual dispersal spectra, M_{-1} and M_{-3}, can be evaluated as [15]

$$E = \frac{M_{-1}}{M_{-3}} \quad \text{and} \quad E_d^2 = \frac{M_{-1}^3}{M_{-3}}. \tag{9}$$

When rearranging (9), one gets

$$M_{-1} = \frac{E_d}{E_o} \quad \text{and} \quad M_{-3} = \frac{M_{-1}}{E_o^2}. \tag{10}$$

Ahmed T. Hassan et al.
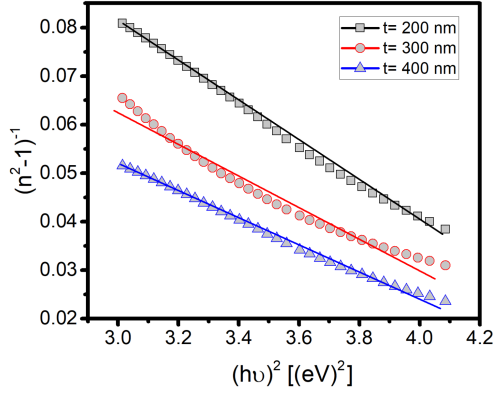
Fig. 5. Plot of $(n^2 - 1)^{-1}$ as a function of $(h\nu)^2$ for Fe_2O_3.
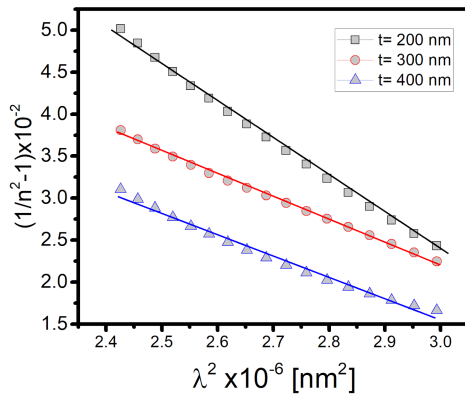
Fig. 6. Dependence of $(n^2 - 1)^{-1}$ on λ^2 for Fe_2O_3.

The obtained M_{-1} and M_{-3} moments replace the thickness. The estimated values of M_{-1} range from 4.89 to 7.48 [dimensionless], and M_{-3} lies between 0.99 and 1.53 eV^{-2}, as shown in Table I. The single-term Sellmeier relationship is given as

$$n^2 - 1 = \frac{S_o \lambda_o^2}{1 - (\frac{\lambda_o}{\lambda})^2}. \tag{11}$$

One can rewrite (11) as follows

$$(n^2 - 1)^{-1} = \frac{1}{S_o \lambda_o^2} - \frac{1}{S_o} \frac{1}{\lambda^2}, \tag{12}$$

where λ_o is the regular oscillator wavelength and S_o is the typical oscillator power. The variables S_o and λ_o in (12) can be estimated with the function $(n^2 - 1)^{-1}$ vs λ^2 and compare to the experimental points, as shown in Fig. 6. The variables S_o and λ_o in (12) can be estimated experimentally by the function $(n^2 - 1)^{-1}$ versus λ^2, as shown in Fig. 6. The slope of the fitted straight line gives $1/S_0$, and the endless capture of the wavelength gives $1/(S_0) \times \lambda_0^2$. The evaluated values of S_0 and λ_0 are given in Table II.

4. Conclusions

Iron oxide Fe_2O_3 thin films of different thicknesses were deposited onto preheated glass substrates by SPT at the temperature of 450°C. The diffraction pattern is polycrystalline, and the crystallization increases as film thickness increases. Noticable shifts occur in the value of the refractive index wavelength, from 2.42 to 2.91, and the energy band gap which drops from 2.74 eV to 2.21 eV. The Urbach energy values rise from 680 to 1230 and dispersal powers rise from 10.86 to 16.54 as the film thickness increases. The changes in these properties are important factors for consideration in potential areas of application of Fe_2O_3 thin films.

References

[1] M.F. Al-Kuhaili, M. Saleem, S.M.A. Durrani, *J. Alloys Compd.* **521**, 178 (2012).

[2] M. Allen, D. Willits, J. Mosolf, M. Young, T. Douglas, *Adv. Mater.* **14**, 1562 (2002).

[3] W.B. Ingler Jr., S.U.M. Khan, *Thin Solid Films* **461**, 301 (2004).

[4] A.S. Hassanien, A.A. Akl, *Appl. Phys. A* **124**, 752 (2018).

[5] B. Ouertani, J. Ouerfelli, M. Saadoun, H. Ezzaouia, B. Bessaïs, *Thin Solid Films* **516**, 8584 (2008).

[6] H.G. Cha, C.W. Kim, Y.H. Kim, M.H. Jung, E.S. Ji, B.K. Das, J.C. Kim, Y.S. Kang, *Thin Solid Films* **517**, 1853 (2009).

[7] J.M.G. Leal, *Phys. Status Solidi B* **250**, 1044 (2013).

[8] A.A. El-Fadl, A.M. Al-Salam, A.M. Nashaat, *Mater. Sci. Poland* **36**, 685 (2018).

[9] M. Fondell, T.J. Jacobsson, M. Boman, T. Edvinsson, *J. Mater. Chem. A* **2**, 3352 (2014).

[10] Q.W. Chen, Y.T. Qian, H. Qian, Z.Y. Chen, W.B. Wu, Y.H. Zhang, *Mater. Res. Bull.* **30**, 443 (1995).

[11] V. Goossens, J. Wielant, S.V. Gils, R. Finsy, H. Terryn, *Surf. Interface Anal.* **38**, 489 (2006).

[12] A. Kumar, K. Yadav, *Mater. Res. Express* **4**, 075003 (2017).

[13] C.M. Tian, W.-W. Li, Y.M. Lin et al., *J. Phys. Chem. C* **124**, 12548 (2020).

[14] G. Neri, A. Bonavita, S. Galvagno, Y.X. Li, A. Trinchi, K. Galatsis, W. Wlodarski, *Sens. Microsyst.*, 149 (2002).

[15] L. Francioso, S. Capone, P. Siciliano, D. Kotsikau, M. Ivanovskaya, *Sens. Microsyst.*, 205 (2008).